Design and experimental tests of free electron laser wire scanners

G. L. Orlandi,* P. Heimgartner, R. Ischebeck, C. Ozkan Loch, S. Trovati,†
P. Valitutti,‡ and V. Schlott
Paul Scherrer Institut, 5232 Villigen PSI, Switzerland

M. Ferianis and G. Penco
Elettra-Sincrotrone Trieste, 34149 Basovizza, Trieste, Italy
(Received 23 March 2016; published 16 September 2016)

SwissFEL is a x-rays free electron laser (FEL) driven by a 5.8 GeV linac under construction at Paul Scherrer Institut. In SwissFEL, wire scanners (WSCs) will be complementary to view-screens for emittance measurements and routinely used to monitor the transverse profile of the electron beam during FEL operations. The SwissFEL WSC is composed of an in-vacuum beam-probe—motorized by a stepper motor—and an out-vacuum pick-up of the wire signal. The mechanical stability of the WSC in-vacuum hardware has been characterized on a test bench. In particular, the motor induced vibrations of the wire have been measured and mapped for different motor speeds. Electron-beam tests of the entire WSC setup together with different wire materials have been carried out at the 250 MeV SwissFEL Injector Test Facility (SITF, Paul Scherrer Institut, CH) and at FERMI (Elettra-Sincrotrone Trieste, Italy). In particular, a comparative study of the relative measurement accuracy and the radiation-dose release of Al(99) : Si(1) and tungsten (W) wires has been carried out. On the basis of the outcome of the bench and electron-beam tests, the SwissFEL WSC can be qualified as a high resolution and machine-saving diagnostic tool in consideration of the mechanical stability of the scanning wire at the micrometer level and the choice of the wire material ensuring a drastic reduction of the radiation-dose release with respect to conventional metallic wires. The main aspects of the design, laboratory characterization and electron beam tests of the SwissFEL WSCs are presented.

DOI: 10.1103/PhysRevAccelBeams.19.092802

I. INTRODUCTION

SwissFEL will provide coherent x-rays light in the wavelength region $7-0.7$ nm and $0.7-0.1$ nm [1]. Electron bunches with charge of 200/10 pC and transverse normalized slice emittance of 0.4/0.2 mm mrad will be emitted by a S-band photocathode gun at a repetition rate of 100 Hz according to a two-bunches structure with a temporal separation of 28 ns. The electron beam will be then accelerated up to 330 MeV by a S-band rf booster and, finally, to 5.8 GeV by a C-band rf linac. Thanks to an off-crest acceleration in the rf booster, the electron beam will experience a longitudinal compression in two magnetic chicanes from an initial bunch length of 3/1 ps (rms) down to 20/3 fs (rms). Two X-band rf cavities will compensate the quadratic distortion of the longitudinal phase space due to the off-crest acceleration of the beam and the nonlinear contribution of the magnetic dispersion [2]. In the booster section, a laser-heater will smooth down possible micro-structures affecting the longitudinal profile of the beam [3,4]. Finally, thanks to a rf kicker—placed after the second bunch-compressor—and a magnetic switch-yard, the second electron bunch of the beam train will be shifted from the main beam line to a secondary one so that the SwissFEL linac, after a further acceleration stage of the two bunches, will supply two distinct undulator chains at a repetition rate of 100 Hz: the hard x-rays line Aramis and the soft x-rays line Athos [1].

In a FEL (free electron laser) driver linac, wire scanners (WSCs) are currently used to monitor the transverse profile of the electron beam [5–13] when the view-screen imaging of the beam is hampered by coherent radiation emission due to microbunching. In SwissFEL, WSCs will be complementary to view-screens for emittance measurements and, thanks to the barely invasive feature, also used for routine monitoring of the transverse profile of the electron beam during FEL operations. Moreover, the beam imaging at SwissFEL being performed by means of YAG:Ce screens [14], only WSCs will be able to discriminate the profile of each single bunch in two-bunches operations. In SwissFEL, the WSC in-vacuum hardware consists of a planar wire fork which can be inserted 45° with respect to the vertical direction into the vacuum chamber by means of a Ultra-High Vacuum (UHV) linear-stage driven by a

*gianluca.orlandi@psi.ch
†Present address: Stanford University—School of Medicine, Stanford, CA, USA.
‡Present address: Australian Synchrotron, Melbourne, Australia.

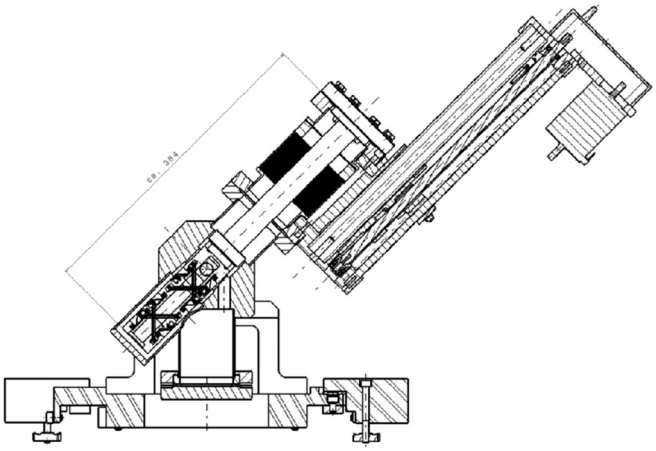

FIG. 1. View of the transverse section of the in-vacuum setup of the SwissFEL WSC: CF16 vacuum chamber, motorized UHV-Linear-Stage and wire fork. The SwissFEL wire-fork can be equipped with two triplets of wires. Thanks to a system of multiple pin slots, the horizontal and the vertical wires of each triplet can be set, respectively, at a distance from the center of the vacuum chamber of either 8 mm or 5.5 mm or 3 mm, see also Fig. 2. In order to outline this feature of the SwissFEL wire-fork—in both Figs. 1 and 2—all the three pin slots are virtually provided with wires. In the real wire-fork of SwissFEL, only one wire is fixed along the horizontal direction by means of one of the three possible pin slots (the same for the vertical direction).

stepper motor, see Fig. 1. The wire-fork is designed to be equipped with two wire triplets, the spare triplet being possibly composed of wires of different material and/or diameter. Each wire of the triplet will separately scan the beam profile along a given direction: the vertical wire (X-scanning, horizontal-scanning), the horizontal wire (Y-scanning, vertical-scanning) and the diagonal wire (XY-coupling). During a WSC measurement, the single wire scanning the beam at a constant speed produces—at every rf shot—a shower of primary scattered electrons and secondary emitted particles in proportion to the fraction of the beam sampled by the wire. In SwissFEL, the forward—high energy and small scattering angle—component of the particle shower (wire signal) will be out-vacuum detected by means of beam loss monitors (BLMs). The beam-loss sensitive material of the SwissFEL BLMs is a scintillator fiber (Saint Gobain BCF-20, decay time 2.7 ns) wrapped around the vacuum pipe. The scintillator fiber is matched by means of a plastic optical fiber (POF) to a photomultiplier (PMT) having a remotely adjustable gain in the range $5 \times 10^3 - 4 \times 10^6$. The PMT signal is finally digitized and integrated in time by an analog-to-digital converter (ADC) unit. The SwissFEL BLMs are designed to detect the wire signal from 10–200 pC bunches and to have a sufficient time-response to discriminate the 28 ns time structure of the SwissFEL beam in two-bunches operations [15]. In SwissFEL, the wire-scanned profile of the electron beam will be reconstructed thanks to the beam-synchronous acquisition (BSDAQ) of the encoder read-out of the wire-position and of the signal read-out of the BLM at every rf shot. Furthermore, thanks to the BSDAQ readout of the beam charge and the transverse position of the beam centroid provided by beam position monitors (BPMs) [16] placed immediately downstream and upstream the WSC, possible errors due to the beam jitter can be corrected in the reconstructed beam profile.

In the present work, technical details on the design of the SwissFEL WSCs will be presented as well as the main results of the bench and electron-beam tests of the entire WSC setup. Laboratory tests aimed at determining the mechanical stability of the in-vacuum hardware of the WSC and, in particular, the stepper-motor induced vibration of the wire in the speed range of interest of SwissFEL were carried out. e-beam tests of a prototype of the SwissFEL WSC—in-vacuum and out-vacuum components—were performed: (1) at low charge and energy—10 pC and 250 MeV—at SITF [17] and (2) at high charge and energy—700 pC and 1.5 GeV—at FERMI [18,19]. Thanks to the e-beam tests, the issue of the necessary detection sensitivity and dynamics of the SwissFEL BLM in the beam charge range 10–200 pC was clarified as well as the issue of the optimum distance of the BLM from the WSC as a function of the beam energy. The question of the choice of the most suitable wire solution (material and diameter) was also positively defined thanks to the e-beam tests. The robustness of wires of different materials and diameters was tested on electron beams. The relative measurement accuracy and the radiation-dose release along the machine during a WSC measurement was also determined for different wire solutions. In particular, a comparative study of the scanning performances—relative measurement accuracy and radiation-dose release—of a $\mathrm{Al(99):Si(1)}$ wire with a diameter of 12.5 μm and a tungsten (W) wire with a diameter of 5 μm was carried out at FERMI at a beam energy of 1.325 GeV and at a charge of 700 pC.

II. DESIGN OF THE SWISSFEL WIRE SCANNERS

In SwissFEL, view screens and WSCs will be used to monitor the transverse profile of electron beams with a size varying between 500 μm and 5 μm (rms) along the entire machine. The fork of the SwissFEL WSC—see Fig. 2—can be equipped with a main triplet of metallic wires and a second spare triplet of wires. Each metallic wire can be fixed between two pins and suitably stretched by means of a metallic spring. Thanks to a system of multiple pin slots, three different distances (8,5.5 and 3 mm) between the wire-vertex of each triplet and the center of the beam pipe can be set and, consequently—for a given motor speed—three different time intervals can be suitably chosen to perform the sequential scanning of the three beam projections.

In the design of the SwissFEL WSCs, particular care was devoted to the choice of the wire material. Several wires of

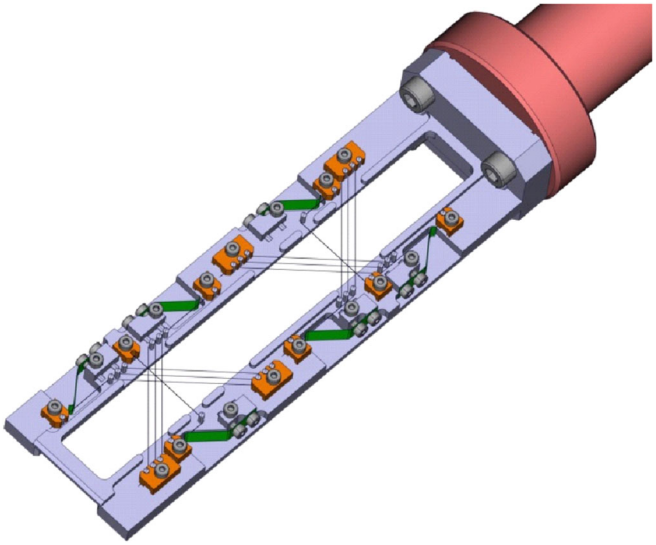

FIG. 2. Technical drawing of the SwissFEL wire-fork. Thanks to a system of multiple pin slots, the vertex of each wire-triplet can be set at three different distances (8,5.5 and 3 mm) from the center of the vacuum chamber. In order to outline such a flexibility feature of the design of the SwissFEL wire-fork—in the present technical drawing—all the three pin slots are shown to be provided with horizontal and vertical wires. In reality, only one of the three possible pin slots will be equipped with a wire so that each of the two wire triplets of the SwissFEL wire-fork will be composed of: one single horizontal wire; one single vertical wire; one single wire for XY coupling.

different material and diameter were indeed tested on the electron beam at SITF and FERMI. The special design of the SwissFEL wire-fork with the possibility to be equipped with two distinct triplets of wires offered the unique opportunity to make simultaneous comparative tests of different wires as described in the following. In SwissFEL, wire scanners will be used to measure the beam emittance by means of a quadrupole scan—an operation normally carried out under undulator protection from the radiation damage due to an unmatched beam transport—as well as to routinely monitor the transverse size of the beam under FEL operations. In the latter WSC application, the radiation-dose release along the machine can be detrimental to critical components of the machine such as the undulators. For such a reason, the choice of wire material and diameter for the SwissFEL WSCs was the object of a careful investigation. The search for the optimum wire solution was not only driven by the constraint to reduce as much as possible the diameter (D) of the wire—$D/4$ being the rms size of the wire defines indeed the rms geometrical resolution in a WSC measurement [20]—but also by the constraint to choose a material with the lowest density (ρ) and atomic number (Z). In fact, the radiation energy losses ΔE of a high energy electron beam with energy E scale down with ρ, Z and the thickness Δx of the material according to the formula

$$\frac{\Delta E}{\Delta x} = \frac{E}{L_R}, \tag{1}$$

where L_R is the radiation length of the material with $1/L_R$ depending quadratically on Z and linearly on ρ [21]. Further aspects being considered in the choice of the wire material were: (1) the breaking risk of the wire due to anomalous vibrations of the wire-fork and (2) the sensitivity of the wire to low-frequency vibrations induced by the stepper motor. In SwissFEL the wire-fork is indeed motorized by a 2-phase stepper motor which may excite possible low frequency vibration eigenmodes of the wire.

According to the experience of several FEL and x-ray facilities such as FLASH and LCLS [9,10,12,13,22], carbon wires are normally preferred to tungsten wires wherever the risk of radiation damage can be a critical issue and/or whenever accuracy and precision are not relevant to a WSC measurement (WSC as a beam-finder). On the other hand, carbon wires are quite rigid and fragile and thus more susceptible than metallic wires to a breaking risk because of an anomalous vibration of the wire-fork. Moreover, contrary to metallic wires, carbon wires can be only fixed and barely stretched onto a wire-fork. Consequently, the risk of exciting an eigenmode oscillation frequency of the wire because of a resonance with a stepper-motor induced vibration of the wire-fork at low frequency is much higher for a carbon wire than for a metallic wire. Such a risk can be avoided or, at least, mitigated when a sufficiently high mechanical tension is applied to the metallic wire fixed between the two pins so that the eigenmode oscillation frequency of the wire can be shifted toward the high frequency region. The option of stretching the wire is available in the wire-fork of the SwissFEL WSCs which is suitably provided with a metallic spring for each wire. Taking into account the aforementioned issues, metallic wires were preferred to carbon wires for the SwissFEL WSC.

In a FEL facility [9,10,13], tungsten wires are typically used for a WSC. Tungsten wires show indeed exceptional properties from the point of view of the beam robustness (melting point, about 3400 °C) and the mechanical strength (tensile strength, about 1900 MPa). Tungsten wires as well as carbon wires [23] are commercially available with a very small diameter—5 μm tungsten wire can be easily found on the market—hence ensuring a high geometrical resolution in a measurement. Moreover, tungsten being characterized by a high values of the density and the atomic number, the reconstruction of a beam transverse profile scanned by a tungsten wire can benefit from a very high signal-to-noise ratio. On the other hand, the high release of radiation-dose along the machine is also the main drawback of using tungsten wires. For such a reason, the possibility to use for the SwissFEL WSC—as an alternative to tungsten—a different metallic wire was investigated keeping in mind the constraint to reduce as much as possible the release of

the radiation-dose along the machine during a WSC measurement. For such a purpose, wires of an aluminium alloy—Al(99):Si(1)—were selected as a possible solution and tested on the electron beam. Compared to a pure aluminium, the Al(99):Si(1) is characterized by a similar melting point (about 600 °C) but a higher tensile strength (about 300 MPa) which is beneficial to the mechanical strength and the elasticity of the wire. Furthermore, compared to tungsten, Al(99):Si(1) has a much lower density and atomic number, hence ensuring a reduction of the radiation-dose release. Electron beam tests of Al(99):Si(1) wires with a diameter of 12.5 μm have been successfully carried out at FERMI at a beam energy of 1.325 GeV and charge of 700 pC. Comparative results of the scanning performances—measurement accuracy of the beam size and collected radiation-dose at the FERMI undulator chain—of a 12.5 μm Al(99):Si(1) wire against a 5 μm W wire are reported in Sec. II C.

A. Test-bench characterization of the SwissFEL WSCs

The reliability of a WSC measurement of the beam profile depends on the measurement accuracy of the relative position of the wire at each machine trigger event [24–26]. For such a purpose, the readout of both the encoder wire-position and the BLM signals will be acquired in SwissFEL according to a BSDAQ mode as well as the readout of adjacent BPMs to correct the measurement by possible errors due to the transverse jitter of the electron beam. The encoder readout of the wire position can be considered reliably provided that the wire vibration during the scan is negligible, i.e., stays within the tolerance limit defined by the geometrical resolution of the scanning wire. The constraint of the mechanical stability was one of the main issues in designing and prototyping the in-vacuum hardware of the SwissFEL WSCs. In particular, the determination of the wire vibration under motion of the UHV linear stage of the SwissFEL WSC was the object of several campaigns of measurements as already documented in [25,26]. In the present work, the results of wire-vibration measurements recently carried out—Summer 2015—on the last and definitive prototype of the UHV linear stage of the SwissFEL WSC will be reported. The UHV linear stage of the SwissFEL WSC—equipped with an incremental optical encoder, end-switches and a homing sensor—is motorized by a 2-phase stepper motor and remotely driven by a motor controller. The coupling of the motor with the wire-fork holder is ensured by a spindle equipped with a ball-screw and a gear-box with a conversion ratio 1:25 (1 spindle revolution corresponds to 25 motor turns and to a lead screw-pitch of 6 mm). The mechanics of the UHV linear stage has been suitably dimensioned to minimize the motor induced wire-vibration and to guarantee a reliable wire-fork motion from the lowest speed limit of 0.1 mm/s up to 3 mm/s that is the maximum speed of interest of WSC measurements in SwissFEL.

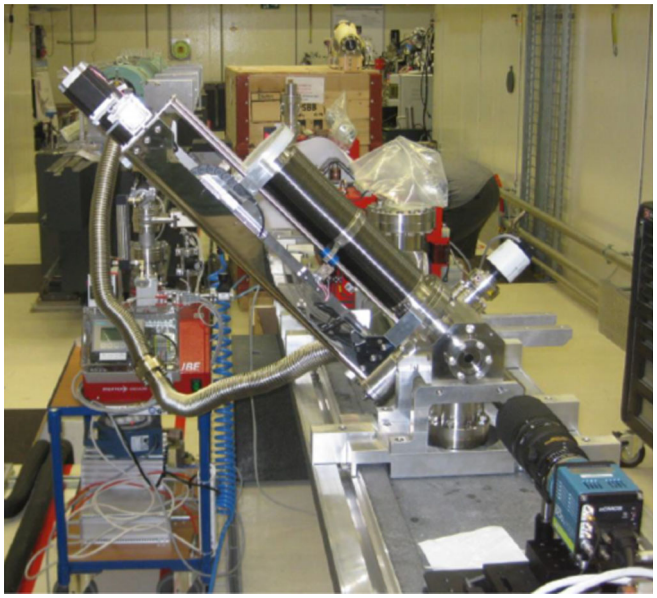

FIG. 3. Image of a prototype of the SwissFEL WSC installed onto a girder together with the measurement setup of the stepper-motor induced vibrations of the wire.

The mechanical stability of the SwissFEL WSC—in particular, the wire stability under stepper motor motion—was characterized by setting up in vacuum—at about 2×10^{-7} mbar—a complete prototype of the system on a SwissFEL girder, see Fig. 3. In Fig. 3, it is possible to recognize the vacuum chamber—mounted on the girder—and the motorized UHV linear-stage which inserts—at 45° into the vacuum chamber—a cylindrical holder with the wire-fork attached, see also Fig. 1. In Fig. 3, it is also possible to recognize a fast camera that is used to image the moving wire. The possible oscillation of the wire is the result of the propagation of the stepper motor induced vibration along the wire-fork and the relative arm. Taking into account the 45° orientation of the wire-fork axis, the horizontal wire mounted at the very bottom of the fork—Fig. 1—is the most critical and sensitive to possible stepper motor induced vibrations. The experimental results shown in Fig. 4 describe indeed the stability features of the horizontal wire mounted at the very bottom of the wire-fork, see Fig. 1. Tungsten (W) wires with a diameter of 25 μm were mounted on the wire-fork and stretched with a sufficient tension to avoid oscillation eigenmodes at a frequency below 1 kHz. Measurements of the wire vibrations induced by the stepper motor were performed by imaging the wire—back-illuminated in the vacuum chamber by a lamp—by means of a sCMOS camera equipped with a 200 mm lens. The motor of the wire-fork was driven in the speed range 0.1–6.0 mm/s. Thanks to a suitable adjustment of the camera ROI (region-of-interest), the camera frame-rate was set to about 565 fps (camera exposure time 1 ms). With a distance between wire and camera ensuring a pixel resolution at the image plane of

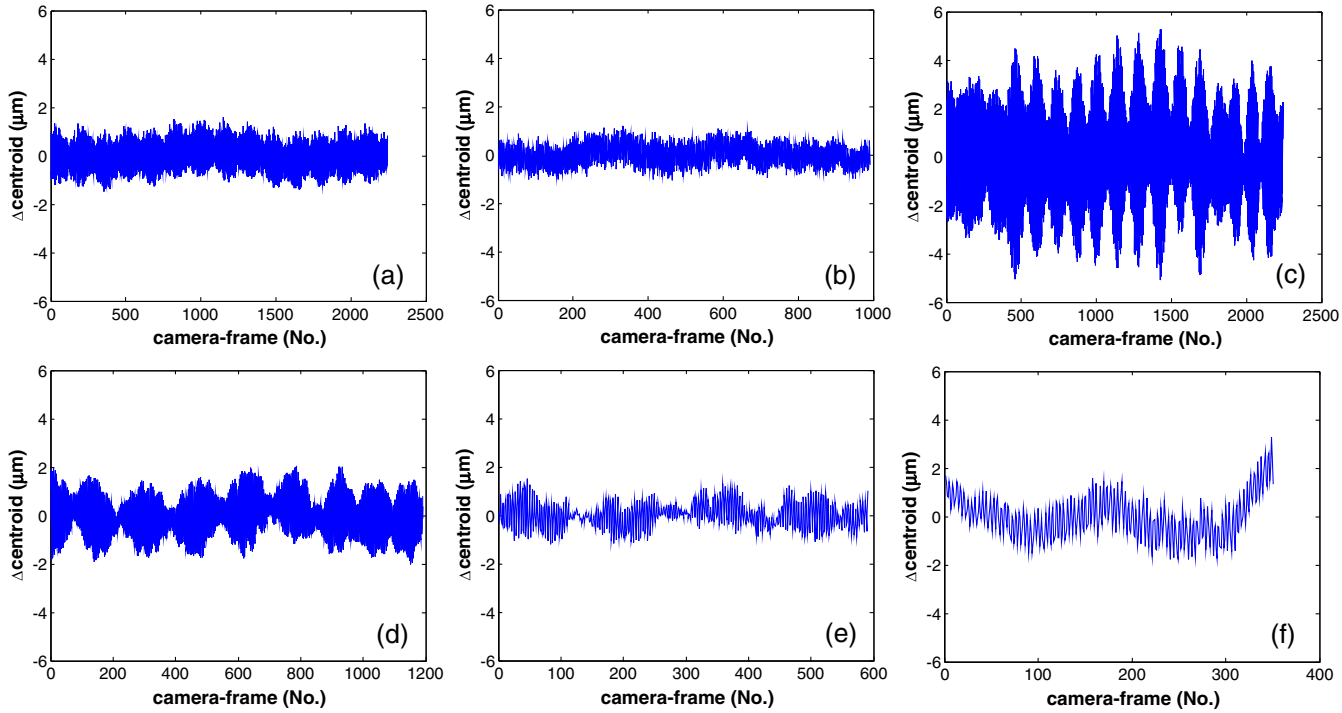

FIG. 4. Measured variations vs time—i.e., vs camera frame number—of the position of the wire centroid—Δ centroid—with respect to the reference value as a function of the motor speed: (a) 0.1 mm/s; (b) 0.4 mm/s; (c) 0.5 mm/s; (d) 1.0 mm/s; (e) 2.0 mm/s; and (f) 3.0 mm/s. The camera frame rate is 565 fps, the camera exposure time is 1 ms.

about 7 μm, the measurement precision of the imaging setup of the wire position was estimated in 0.9 μm (rms) as resulting from the determination of the centroid position of the wire at rest. Thanks to such a measurement precision, it was possible to observe and characterize vibrations of the wire centroid with an accuracy better than the tolerance limit of 1.3 μm which is the rms geometrical resolution achievable in a WSC measurement by a wire with a diameter of 5 μm. The outcome of this measurement campaign of the wire motion confirmed that the vibration of the wire centroid largely remains within a tolerance limit of 1.3 μm (rms) in the motor-speed range 0.1–3.0 mm/s with the exception of a small velocity range 0.5–0.6 mm/s where an anomalous wire vibration of 2.1–1.6 μm slightly exceeding the tolerance limit was observed, see Fig. 4. Meanwhile, the measured diameter (rms) of the moving wire was observed not to vary appreciably with respect to the wire at rest so indicating that the wire does not vibrate at a frequency higher than the characteristic acquisition frequency of the camera (565 fps). In conclusion, taking into account that the motor-speed range of interest of SwissFEL is 0.1–0.3 mm/s at a repetition rate of 10 Hz and 1.0–3.0 mm/s at a repetition rate of 100 Hz—corresponding in both cases to a wire-step of 7.1–21.2 μm per rf shot—the slightly anomalous resonant vibration of the wire observed in the motor-speed range 0.5–0.6 mm/s is definitely not detrimental to a WSC measurement in SwissFEL.

As a further and final comment on the measured wire-vibrations plotted in Fig. 4, the spectral analysis of the measured data of the wire vibrations vs time for different motor speeds was observed to show an amplitude peak at a characteristic frequency of about 150 Hz. An amplitude peak at the same frequency results from the spectral analysis of the measurement vs time of the centroid position of the wire at rest. Consequently, the hypothesis that the wire be affected by a real oscillation mode at this characteristic frequency can be excluded. The observation of this characteristic frequency in the measured data can be interpreted as a spurious effect due either to an environment induced vibration of the entire experimental setup (WSC in-vacuum hardware and camera setup) or to a characteristic vibration of the imaging setup (camera vibration induced by the internal cooling system, time-fluctuation of the light intensity of the lamp joined to a nonhomogeneous spatial distribution of the light over the camera field of view).

B. e-beam tests of the SwissFEL WSCs at SITF

Several WSC tests were carried out at SITF [17] until Fall 2014 when the decommissioning of the test facility started. The experimental activity at SITF dealt with: comparison—WSC against view-screen—of beam transverse profile measurements; beam resistance tests of tungsten wires of different diameters; determination of

the optimum distance between WSC and BLM at a beam energy of a few hundred MeV; study of the BLM sensitivity and detection dynamics in the beam charge range 10–200 pC and of the detector capability to discriminate the 28 ns time-structure in two-bunches operations.

The very first prototype of the WSC installed at SITF was composed of a wire-fork extension integrated in the view-screen holder, see Fig. 5. The insertion axis of this WSC prototype being vertical, only the horizontal wire was used for a direct measurement of the vertical profile of the electron beam. At the early stage of the beam operations at SITF, BLMs were not available. Consequently, the detection of the wire-signal during a WSC measurement was obtained as the differential charge read-out of a first BPM placed upstream the WSC and of a second BPM placed downstream the WSC in the arm of the high energy spectrometer of the linac. Since a portion of the wire-signal (primary scattered electrons and secondary emitted electrons) does not match the energy acceptance of the high energy spectrometer, a differential measurement of the charge readout of the two aforementioned BPMs provides a relative measurement of the fraction of the beam charge intercepted by the wire at each rf shot. The BSDAQ at 10 Hz of the charge readout of the two BPMs and of the encoder readout of the wire position during a wire-scan allowed the vertical profile of the electron beam to be reconstructed. Measurements of the vertical profile of the electron beam with a size in the range 0.1–0.9 mm (rms) were carried out at SITF [26] by means of an OTR screen and a coaxial WSC at a beam charge of 160 pC and energy of 230 MeV as shown Fig. 6. According to a linear fit of the experimental data plotted in Fig. 6, the relative measurement accuracy of a WSC against an OTR screen stays within 2% in the vertical beam size range 0.1–0.9 mm.

Other issues to be clarified to complete the design of the SwissFEL WSC dealt with: (1) the feasibility of the out-vacuum detection of the forward component of the particle shower produced in a WSC measurement; (2) the determination of the optimum distance between WSC and BLM as a function of the beam energy; (3) the sensitivity of the SwissFEL BLM in detecting a wire-signal from a 10 pC bunch.

Numerical simulations of the angular and energy distribution of the particle shower produced by an electron beam intercepting a tungsten wire with a diameter of 13 and 25 μm were performed by means of the Monte Carlo code FLUKA [26–28]. The electron beam was modeled as a pencil beam (no energy spread) with energy 0.340, 1.330, 2.990 and 5.200 GeV traveling along the symmetry axis of the vacuum chamber. According to the results of the simulations, primary and secondary electrons mainly compose the particle shower which, for a fraction of about 95%, is forward emitted with a uniform energy distribution within a polar angle of $\pi/16$ rad with respect to the beam axis, see Figs. 7 and 8. In conclusion, based on a very simplified model of the machine which does

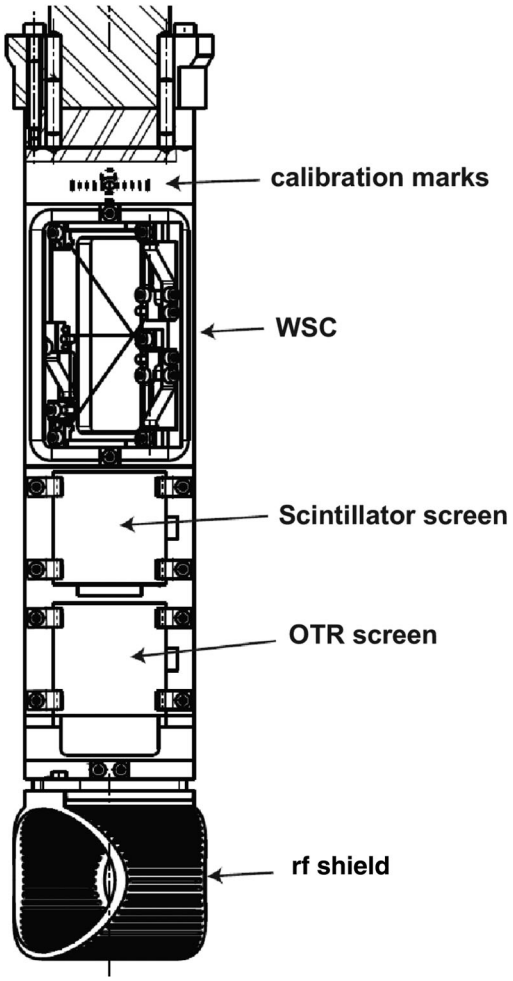

FIG. 5. Technical drawing of the SITF view-screen holder with the integrated WSC extension.

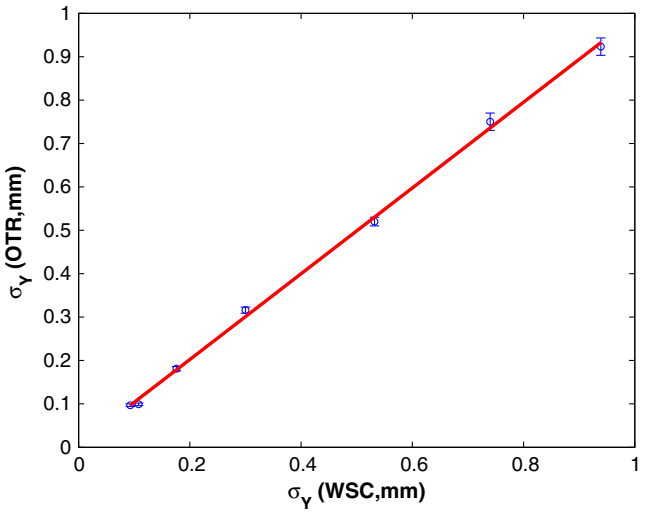

FIG. 6. Comparison OTR against WSC of beam profile measurements. The relative accuracy of a WSC measurement against OTR is within 2%. Beam energy 230 MeV, beam charge 160 pC.

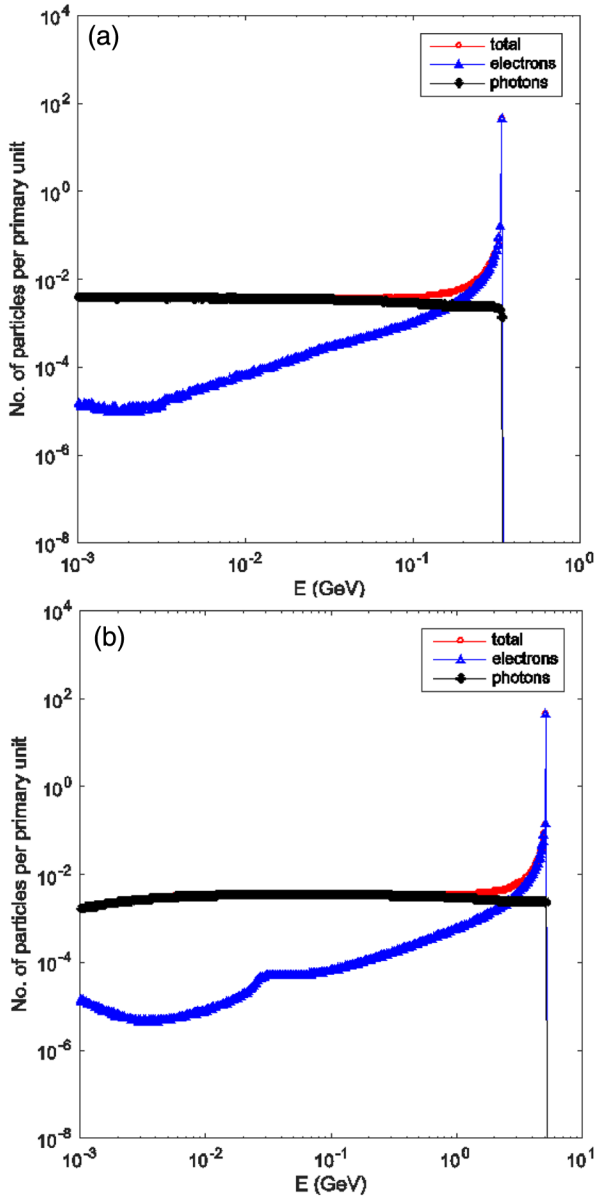

FIG. 7. Energy distribution of the main components of the particle shower forward emitted in the polar angle $0 - \pi/16$ rad by an electron beam with energy 0.340 (a) and 5.2 (b) GeV colliding onto a 13 μm tungsten wire.

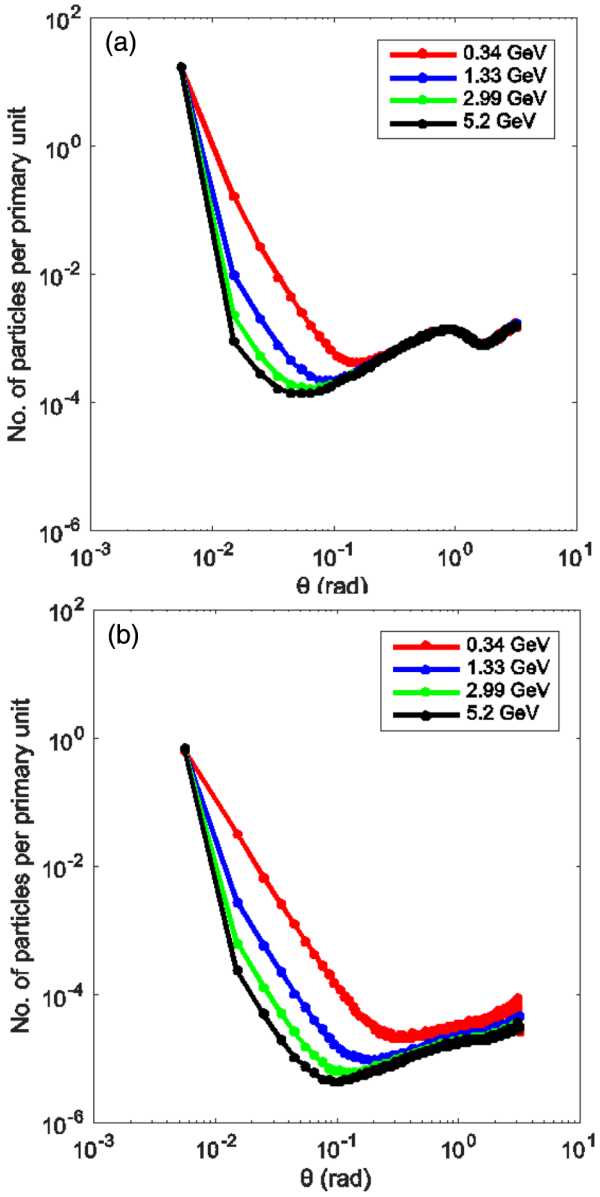

FIG. 8. Number of electrons (a) and photons (b) forward emitted in the collision of an electron beam with a 13 μm tungsten wire as a function of the polar angle (rad) per primary incident particle for different beam energies: 0.340, 1.33, 2.99 and 5.2 GeV.

not include any magnetic shaping and rf transport of the wire-scattered beam, FLUKA simulations predict that about 95% of the wire-signal intercepts a CF16 vacuum-pipe—inner and outer diameter 16 and 18 mm, respectively—at a distance from the wire roughly between 0.1 and 4.0 m.

A first experimental check of this numerical prediction of the optimum distance WSC-BLM was carried out at SITF. For such a purpose, a BLM monitor was installed at the very end of SITF just in front of the dipole of the high energy spectrometer. After setting a full charge transport of the electron beam—energy 245 MeV and charge 180 pC—up to the beam dump of SITF, the electron beam was then alternatively fully intercepted by means of the single OTR screens (0.1 μm Al coating on a 300 μm thick Si wafer)—see Fig. 5—which were available along the beam line. Meanwhile, at each OTR screen insertion, the corresponding BLM readout was recorded as shown in Fig. 9 where the BLM readout vs distance from the inserted OTR screen is plotted. According to a rule-of-thumb extrapolation—based on Eq. (1)—from the data shown in Fig. (9), for a WSC equipped with 5–10 μm tungsten wires, a maximum of the BLM signal can be expected at a distance from the WSC of about 2.5–3 m at a beam energy of about 250 MeV. This result being in agreement with the simulation prediction [28] of the optimum distance WSC-BLM also

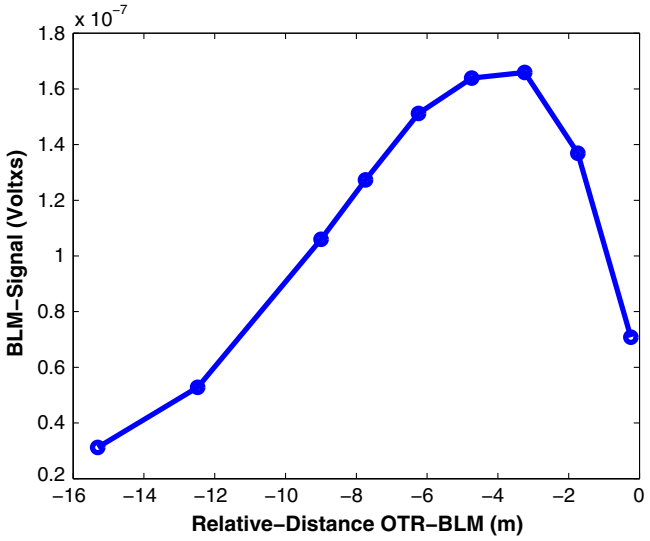

FIG. 9. BLM readout as a function of the distance of the OTR screen intercepting the electron beam. Beam energy and charge: 245 MeV and 180 pC.

complies with the outcome of analogous measurements previously carried out at SITF with a different detection setup and different screens [29] (LuAG:Ce scintillator instead of OTR screen) and with the results of further WSC measurements described in the following. As a conclusion of this measurement session, the vertical profile of the electron beam at SITF was measured by means of an OTR screen and the related coaxial WSC—see Fig. 10—both placed at the optimum distance of about 3 m from the BLM.

The first beam test of the in-vacuum hardware of the SwissFEL WSC—see Fig. 1—was carried out at SITF in Summer 2014. Goals of this first experimental test of the hardware of the SwissFEL WSC at SITF was the study of the (1) signal response of the beam loss monitor (BLM) when scanning a 10 pC beam with a 5 μm tungsten wire and of the (2) optimum distance WSC-BLM at a beam energy of about 200 MeV. The wire-fork of this WSC prototype was equipped with 5 and 13 μm tungsten wires. Several SwissFEL BLMs were also installed at different distances from the WSC: BLM1 at 0.6 m (just at the junction of the vacuum-pipe with the WSC vacuum-chamber), BLM2 at 2.3 m and BLM3 at 3.5 m. Since only two electronic boards of the PMT signal were available at that time, the simultaneous readout of only two BLMs was possible. Therefore, in two distinct WSC measurement sessions—beam energy of 200 MeV and charge of 10 and 200 pC—the signals of both BLM1

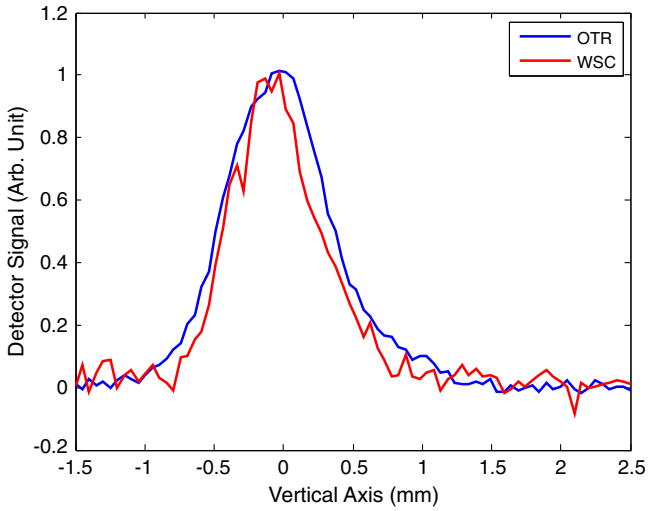

FIG. 10. Vertical profiles of the electron beam—energy 245 MeV and charge 180 pC—resulting from the projection of an OTR image and from a WSC measurement of the beam: $\mathrm{sigma(OTR, rms)} = (0.308 \pm 0.008)$ mm, $\mathrm{sigma(WSC, rms)} = (0.304 \pm 0.014)$ mm. Motor-speed 0.2 mm/s.

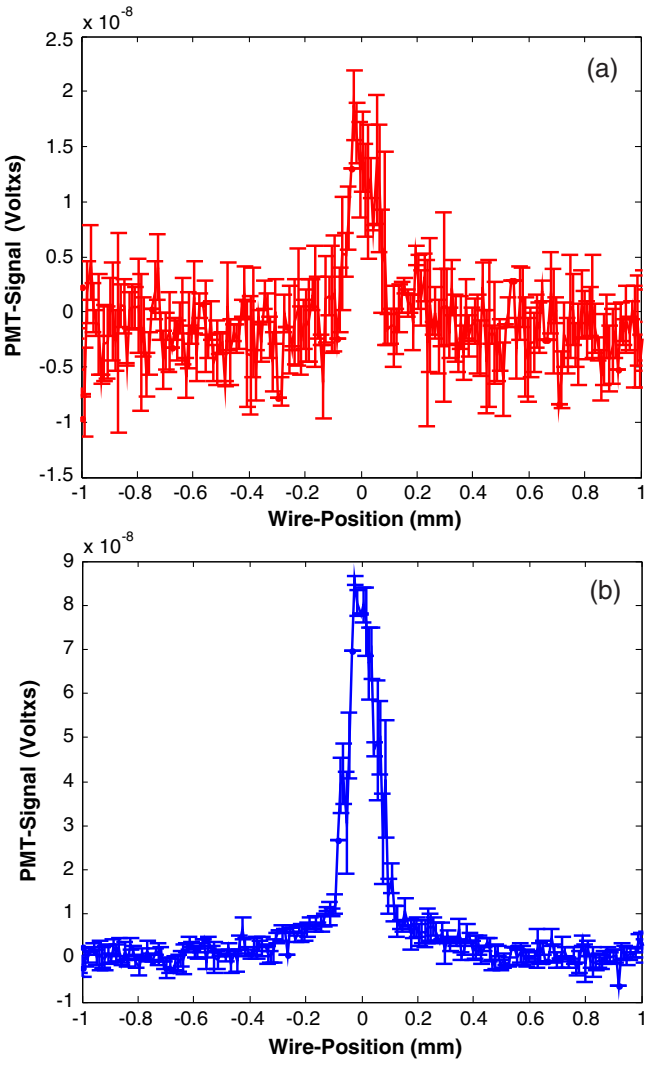

FIG. 11. Beam profile of a 10 pC beam—and energy 200 MeV—scanned by a 5 μm tungsten wire as reconstructed by the signal readout of (a) BLM1 and (b) BLM2 at a distance of 0.6 and 2.3 m from the WSC, respectively.

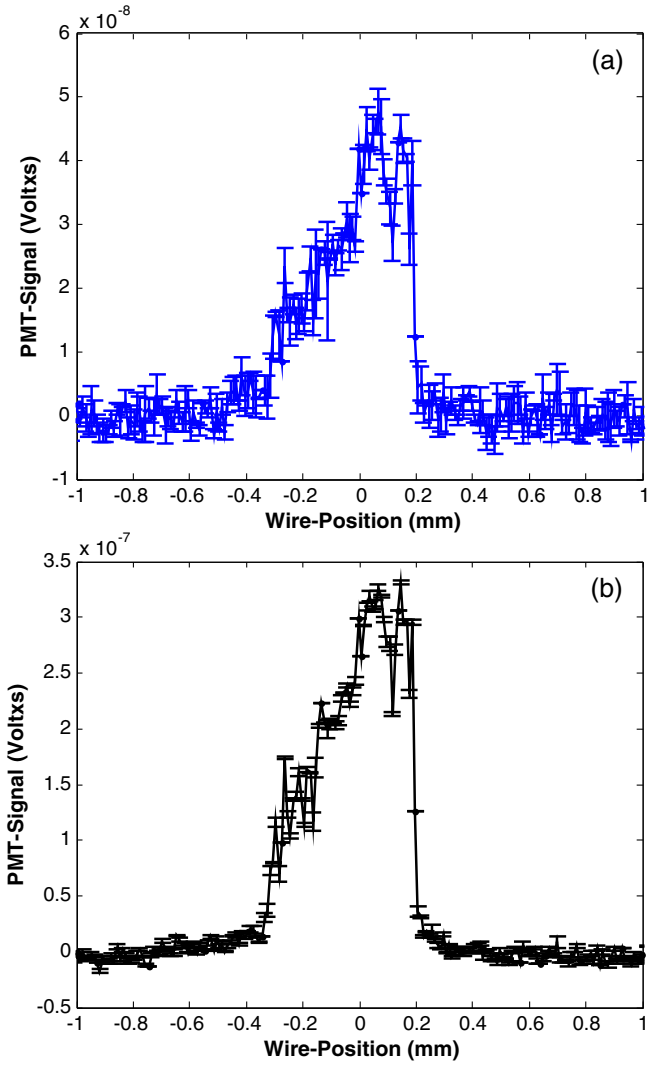

FIG. 12. Beam profile of a 10 pC beam—and energy 200 MeV—scanned by a 5 μm tungsten wire as reconstructed by the signal readout of (a) BLM2 and (b) BLM3 at a distance of 2.3 and 3.5 m from the WSC, respectively.

and BLM2 and both BLM2 and BLM3 were simultaneously acquired, respectively. The results of the scan of a 10 pC beam with a 5 μm tungsten wire being more relevant and meaningful—see Figs. 11 and 12—will be reported hereunder. Data in Fig. 11 were measured by BLM1 (at 0.6 m) and BLM2 (at 2.3 m), while data in Fig. 12 by BLM2 (at 2.3 m) and BLM3 (at 3.5 m). The signal from each BLM has been normalized in proportion to the corresponding value of the PMT gain. Thus, the signal intensities of the beam profiles shown in Figs. 11 and 12 are comparable and indicative of the longitudinal intensity distribution of the wire signal. Since the experimental data shown in Figs. 11 and 12 belong to two different measurement sessions, they are not meaningful from the point of view of the beam size—which is not a relevant parameter in the present context anyhow, the beam size changing from a session to the other and the beam profile in Fig. 12 being clearly not Gaussian—but they can provide useful information about the BLM sensitivity and about the longitudinal distribution of the wire-signal intensity. From the comparative analysis of the signal detected by the three BLMs, a maximum of the wire-signal intensity was observed at the position of BLM3, i.e., at a distance of 3.5 m from the WSC. At a distance of 0.6 m from the WSC, the beam losses resulting from a 10 pC beam scanned by a 5 μm tungsten wire were barely sufficient to measure a size of a few tens of μm. As an outcome of this experimental test, the sensitivity of the SwissFEL BLM is sufficient to detect wire signals resulting from the scan of a 10 pC beam with a 5 μm tungsten wire. In addition, a further confirmation that the optimum distance WSC-BLM is expected to be around 3 m at a beam energy of 250 MeV can be drawn. Tests of the SwissFEL BLM in two-bunches operations were also carried out at SITF.

C. e-beam tests of the SwissFEL WSCs at FERMI

The experimental tests carried out at SITF—decommissioning started end 2014—could not give an answer to all the open issues of the design of the SwissFEL WSC. After the SITF experience, the suitability of the proposed detection technique of the wire signal at the GeV energy scale still needed to be verified as well as the scaling rule of the optimum distance between WSC and BLM as a function of the beam energy. Furthermore, the study of new wire materials would have taken advantage of possible beam tests at high energy and charge. On the basis of these motivations, a collaboration with FERMI started. A prototype of the in-vacuum component of the SwissFEL WSC—vacuum-chamber, UHV linear-stage and wire-fork—was installed at FERMI in the beam transport line from the linac to the undulator beam line just after the high energy spectrometer, see Figs. 13 and 14. Three SwissFEL BLMs were also installed at a distance from the WSC of 2.48, 5.52 and 8.40 m, respectively. In particular, two BLMs were installed in the linac hall while a third one was installed in the undulator hall just behind the beam-stopper and a concrete wall separating the two halls. The light signal of each scintillator fiber—being transferred via a POF to the technical gallery—is converted to an electrical signal by a PMT having a variable gain. The PMT signal is finally digitized by a VME multichannel ADC board running at 250 Msamples/s.

Two series of experimental tests of the SwissFEL WSC were carried out at FERMI. In the first one, the wire-fork was equipped with two couples of tungsten wires with a diameter of 13 and 5 μm, respectively. In the second one, the wire-fork was equipped with a couple of 5 μm tungsten wires and a couple of 12.5 μm Al(99):Si(1) wires. Each couple of wires was composed of one horizontal wire for the measurement of the vertical profile of the electron beam

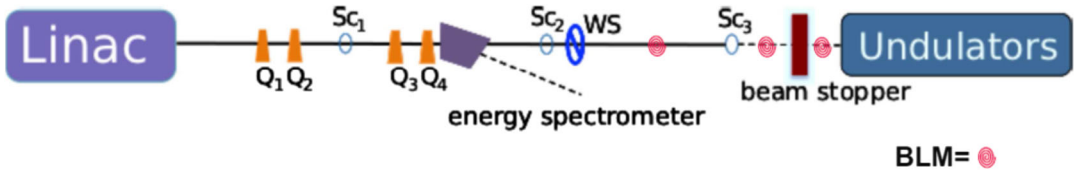

FIG. 13. Schematic layout of FERMI and of the SwissFEL WSC and BLM setup. In the picture, the WSC is indicated as WS while the BLM are represented as a red spiral. Quadrupoles Q_j $(j = 1, \ldots, 4)$ and view-screens Sc_i $(i = 1, \ldots, 3)$ used at FERMI for emittance measurements are also sketched.

and one vertical wire for the measurement of the other orthogonal projection of the electron beam.

The first WSC test at FERMI—beam energy 1.5 GeV, charge of 300 pC, repetition rate 10 Hz—aimed at checking the robustness of a 5 μm tungsten wire and determining the optimum distance between WSC and BLM at the GeV energy scale. Beam profiles—as measured by the three aforementioned BLMs—during a scan with a 5 and a 13 μm tungsten wire are shown in Figs. 15(a,b) and in Figs. 15(c,d), respectively. The data plotted in Figs. 15(a,c) refer to the horizontal profile of the electron beam ($\sigma = 53$ μm rms, 2% statistical error), while the data in Figs. 15(b,d) are related to the vertical profile of the electron beam ($\sigma = 80$ μm rms, 2% statistical error). The signals of the three BLMs plotted in Figs. 15 being absolute values are comparable in order to evaluate how the wire-signal strength varies along the beam line. According to the analysis of the signal intensity of the three BLMs—see Figs. 15—the optimum location of the BLM can be estimated at a distance from the WSC of about 5–6 m for a beam energy of 1.5 GeV. Furthermore, the observation of a wire signal still appreciable at more than 8 m from the WSC and after a massive obstacle (concrete wall and beam-stopper)—which suppresses or, at least, strongly reduces the particle shower passing from the linac to the undulator hall of FERMI—is reassuring about the possibility to detect the wire signal at a long distance from the WSC whenever this option is mandatory in particular machine sections or setups.

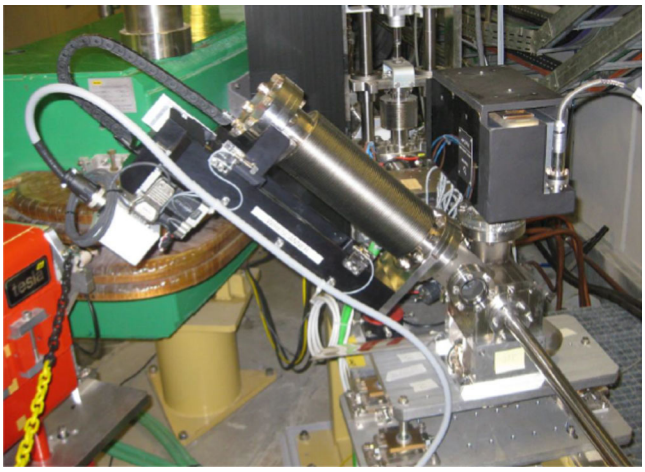

FIG. 14. Picture of the installation of the SwissFEL WSC at FERMI. The WSC in-vacuum hardware is placed in the linac hall just after the dipole of the FERMI high energy spectrometer.

The ratio of the radiation-dose measured by the three BLMs—BLM(1), BLM(2) and BLM(3)—during the wire-scan measurements performed with the 5 and a 13 μm tungsten wires—see measured beam profiles in Fig. 15—is shown in Table I. According to the measured values shown in Table I, the ratio of the integrated signals detected by BLM(2) and BLM(3)—which are 5.52 and 8.40 m far from the WSC, respectively—is similar and consistent with the prediction that is obtainable from Eq. (1) describing the radiation energy losses of a high energy beam interacting with a material of a given thickness Δx. According to Eq. (1), for a given beam energy E, the radiation energy losses resulting from the interaction of a high energy electron beam with a given material scales up with the thickness of the material. Consequently, according to Eq. (1), the expected ratio of the radiation energy losses of a 13 μm tungsten wire to a 5 μm tungsten wire is $13/5 = 2.6$ in agreement with the data measured by BLM(2) and BLM(3), see Table I. The difference between the ratio of the radiation dose measured by BLM(1) and the ones measured by BLM(2) and BLM(3) as well can be explained by the circumstance that BLM(2) and BLM(3) are placed at distances—5.52 and 8.40 m, respectively—from the WSC which make them more suitable than BLM(1) in detecting the high energy—and small scattering angle—component of the wire signal. BLM(1) being closer to the WSC—only 2.48 m away—is more sensitive to the low energy—large scattering angle—component of the particle shower produced in the interaction of the primary electron beam with the wire. Moreover, in the FERMI setup, BLM(1) is only separated from the WSC by a drift space, while several quadrupoles—not plotted in the sketch of Fig. 13—are placed in between the WSC and BLM(2) and BLM(3). Consequently, these quadrupoles play the role to filter the low energy component of the wire signal out of the vacuum chamber while getting most likely confined into the vacuum chamber the high energy component of the wire signal. The higher the energy of the wire signal—primary scattered electrons and secondary emitted electrons—and the smaller the corresponding scattering angle, the higher the probability that the wire signal be transported by the magnetic optics far away from the WSC inside the beam pipe. Consequently, for a high energy electron beam, the

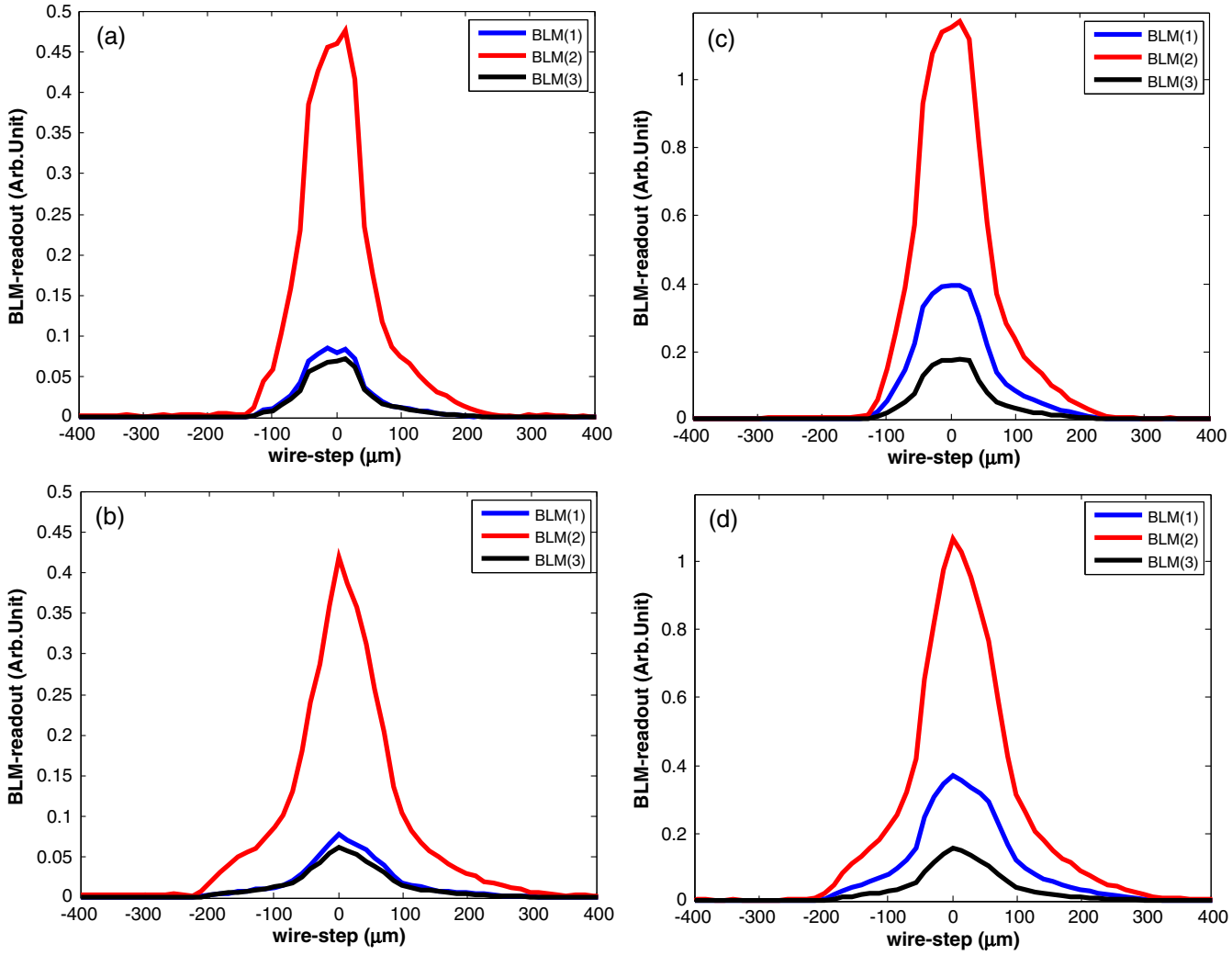

FIG. 15. Horizontal—(a,c) and vertical—(b,d)- wire-scanned profiles of the FERMI electron beam (1.5 GeV, 300 pC). In each figure, signals from the three BLMs placed at different distances from the WSC are plotted: BLM(1) at 2.48 m, BLM(2) at 5.52 m and BLM(1) at 8.40 m. Experimental data in (a,b) results from a scan with 5 μm tungsten wire, while data (c,d) from a scan with a 13 μm tungsten wire. The scan was performed at a wire-fork speed of 0.20 mm/s corresponding to a wire-step of 0.14 mm per rf shot at the machine repetition rate of 10 Hz. The measured beam size in the horizontal and vertical directions is $\sigma = 53$ μm and $\sigma = 80$ μm (rms), respectively, with a statistical error of about 2%.

TABLE I. Ratio of the radiation-dose measured at FERMI by BLM(1), BLM(2) and BLM(3) when scanning with 5 μm and 13 μm tungsten wires—at a motor speed of 0.2 mm/s—the horizontal (Hor) and the vertical (Ver) profiles of a 300 pC electron beam (energy 1.5 GeV, 10 repetition rate). The values of the radiation-dose measured by the three BLMs at every scan were obtained by integrating the beam profiles plotted in Fig. 15. The relative distances from the WSC of the three beam-loss monitors BLM(1), BLM(2) and BLM(3) are: 2.48, 5.52 and 8.40 m, respectively.

	BLM(1)	BLM(2)	BLM(3)
Ratio(W13 μm/W5 μm, Ver)	5.5	2.7	2.5
Ratio(W13 μm/W5 μm, Hor)	5.4	2.7	2.6

scaling rule of the radiation-dose measured by a BLM placed at a long distance from the WSC should be reasonably given by Eq. (1) as the experimental data shown in Table (I) are indicating. Further measurements carried out at FERMI—as in the following described—confirm such an interpretation.

A campaign of emittance measurements aiming at comparing the performance of a WSC with respect to a view-screen was also carried out at FERMI [30]. It resulted that a better accuracy in measuring the beam emittance can be achieved by using WSC as well as a more reliable and efficient matching of the magnetic optics to the design lattice (especially for a beam size of a few micrometers). Further outcome of this first WSC

experience at FERMI was the observation that a wire-scanning—with a 5 and 13 μm tungsten wire at a motor velocity of 0.2 mm/s—is only barely perturbing the FEL emission process and, consequently, it can be routinely performed for on-line monitoring of the beam profile during FEL operations [30].

A second series of WSC tests was performed at FERMI after substituting the previous wire-fork with a new one equipped with a couple of 5 μm tungsten wires and a new wire solution. The new wire solution—new solution for WSC diagnostics, at least—consists of a couple of Al(99) : Si(1) wires with a diameter of 12.5 μm. This second series of WSC tests at FERMI aimed at: first of all, checking suitability and robustness of the Al(99) : Si(1) wires at a high beam energy and charge; then, determining the relative measurement accuracy of an Al(99) : Si(1) scan against a W scan; finally, quantifying the possible reduction of the radiation-dose release of an Al(99) : Si(1) wire scan in comparison with a tungsten wire scan. This comparative study Al(99) : Si(1) vs W was carried out at the FERMI linac which was set and tuned at a stable beam condition—energy 1.325 GeV, charge 700 pC and repetition rate 10 Hz—and at a fixed and matched magnetic optics. For different motor-speeds (0.1, 0.2 and 0.3 mm/s) 10 wire-scans of the beam were performed with a 5 μm tungsten wire and repeated with the homologous 12.5 μm Al(99) : Si(1) wire. At every scan, beam losses were measured at different locations with different detectors: with BLM1 (scintillator fiber placed at a distance of 2.48 m from the WSC), with 2 Cerenkov fibers (Cerenkov1&2) stretched along the beam pipe of the FEL1 undulator beam-line and, finally, with 8 Ionization-Chambers—I-C(1 → 8)—placed in front, at the end and in between the 7 undulators composing the FEL1 undulator chain [31]. Experimental results of the comparative study Al(99) : Si(1) vs W are shown in Figs. 16–19. In Fig. 16, the profile of the electron beam resulting from the beam-losses measured by BLM1 during the scan with two homologous Al(99) : Si(1) and W wires moving at a motor-speed of 0.2 mm/s is shown. The measured values of the beam size resulting from the analysis of the beam losses plotted in Fig. 16—for a motor-speed of 0.2 mm/s—and from the analysis of other experimental beam profiles similarly acquired for motor-speeds of 0.1 and 0.3 mm/s are shown Fig. 17. According to the experimental data plotted in Fig. 17, the same accuracy—within the limit of the statistical errors—is achieved by a 12.5 μm Al(99) : Si(1) and a 5 μm W wire in measuring a beam profile with a size of about 35 μm. Furthermore, within the limit of the statistical errors, the measurement accuracy maintains constant in the motor-speed range 0.1–0.3 mm/s.

Further goal of this WSC measurement session was to quantify the radiation-dose released along the machine when scanning—at different motor speeds—the electron beam with W and Al(99) : Si(1) wires. The relative values of the radiation-dose measured by the detectors BLM1 and

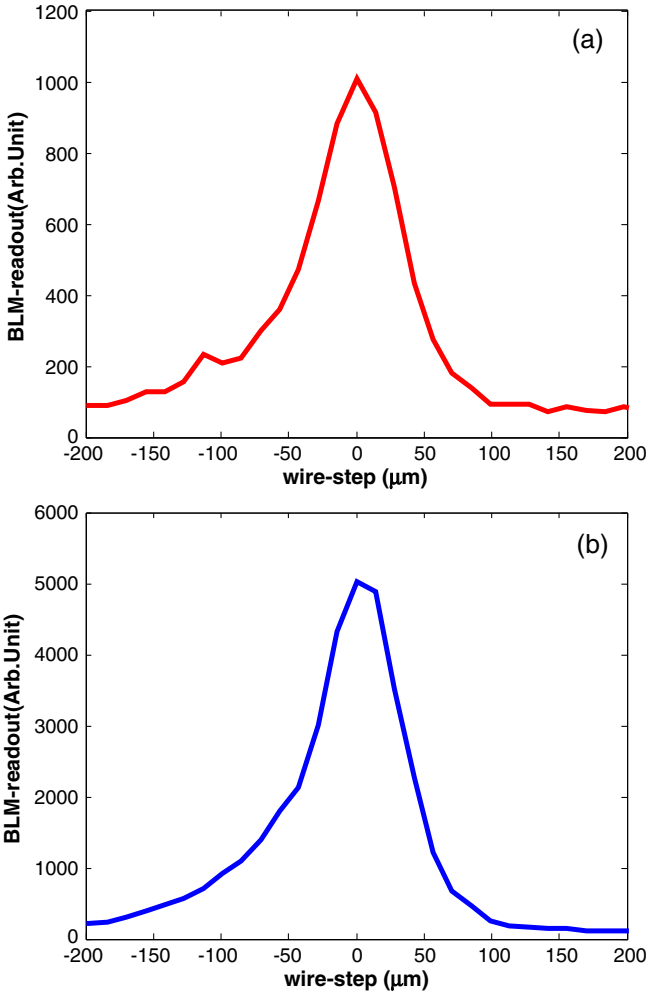

FIG. 16. Beam profile resulting from the scan of the FERMI electron beam with a 12.5 μm Al(99) : Si(1) wire (a) and a 5 μm W wire (b) as detected by a BLM placed at a distance of 2.48 m from the WSC. The scan was performed at a motor-speed of 0.2 mm/s and at a beam energy of 1.325 GeV, charge 700 pC and 10 Hz repetition rate.

Cerenkov1&2 and the absolute values of the radiation-dose rate (mGy/h) measured by the 8 Ionization-Chambers I-C (1 → 8) when scanning the beam with two homologous Al(99) : Si(1) and W wires at a motor speed of 0.2 mm/s are shown in Table II. In Table II, the ratio—W against Al(99) : Si(1)—of the measured values of the radiation-dose are shown as well. In particular, the absolute radiation-dose rate (mGy/h) measured by the 8 Ionization-Chambers of the FERMI FEL1 when scanning—at a motor speed of 0.2 mm/s—the beam with two homologous wires [5 μm tungsten and 12.5 μm Al(99) : Si(1)] is plotted in Fig. 18. According to the results shown in Table II and in Fig. 18, the radiation-dose rate measured by the 8 I-Cs of FERMI FEL1 when scanning the electron beam with a 12.5 μm Al(99) : Si(1) at a motor speed of 0.2 mm/s is a factor 11 smaller than the value measured in a scan with a 5 μm tungsten wire. A reduction by a factor 11 of the radiation-dose

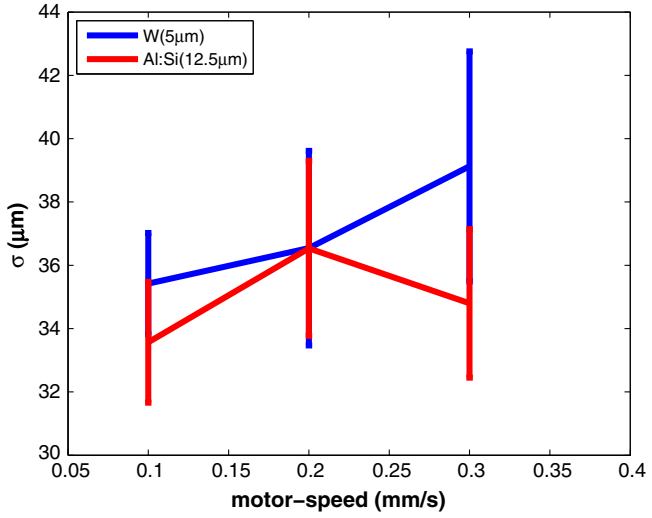

FIG. 17. Beam size measurements resulting from a wire-scan of the FERMI electron beam performed with two homologous 12.5 μm Al(99):Si(1) and a 5 μm W wires. During the measurement, the FERMI machine was set at stable and fixed beam conditions: 1.325 GeV, 700 pC and 10 Hz repetition rate. The WSC measurements of the beam profile were repeated for different motor-speeds: 0.1, 0.2 and 0.3 mm/s.

released along the undulator chain of FERMI FEL1 was also observed at motor-speeds of 0.1 and 0.3 mm/s as shown in Table III where the ratio—W against Al(99):Si(1)—of the absolute values of the radiation-dose rate measured by the 8 I-Cs are shown together with analogous results obtained from the other beam loss monitors. Finally, the radiation-dose rate measured by the 8 I-Cs during the scan of the electron

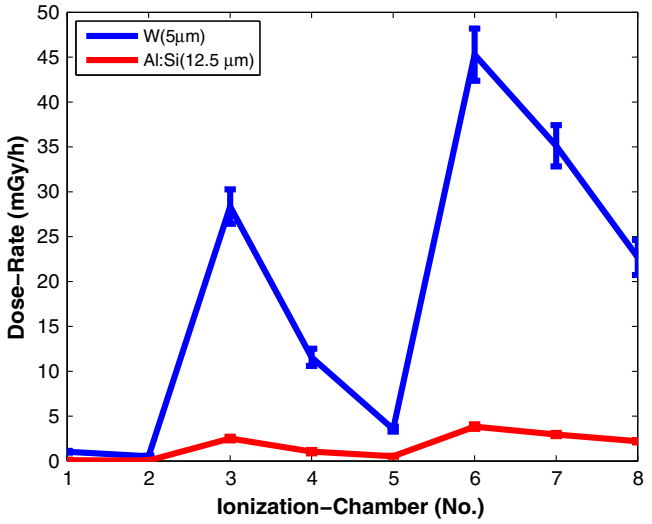

FIG. 18. Average radiation-dose rate (mGy/h) measured by the 8 ionization chambers (I-C) placed in the FERMI FEL1 undulator chain when scanning with 12.5 μm Al(99):Si(1) wire and a 5 μm tungsten wire—at a motor speed of 0.20 mm/s—an electron beam of 700 pC and energy of 1.325 GeV. The data in the plot result from the average—over 10 scans—of the dose-rate readout of the I-Cs integrated over 30 beam shots.

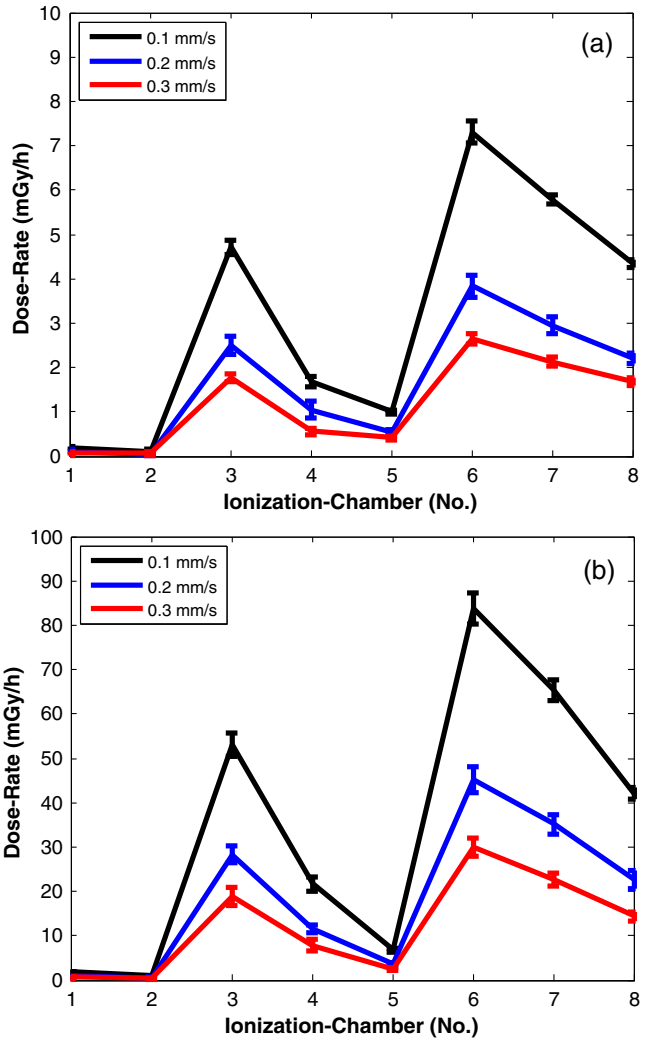

FIG. 19. Average radiation-dose rate (mGy/h) measured by the 8 ionization chambers (I-C) placed in the FERMI FEL1 undulator chain when scanning—with (a) a 12.5 μm Al(99):Si(1) wire and (b) a 5 μm tungsten wire—an electron beam of 700 pC and energy of 1.325 GeV at a motor speed of 0.10, 0.20 and 0.30 mm/s. The data in the plot are the result of the average of the I-C dose-rate readout over 10 scans.

beam with two homologous 12.5 μm Al(99):Si(1) and 5 μm tungsten wires are compared in Fig. 19 for different motor-speeds (0.1, 0.2 and 0.3 mm/s).

About the ratio of the radiation-dose measured by the three different detectors—BLM1 and Cerenkov1&2 and the 8 Ionization-Chambers I-C(1 → 8)—during the comparative WSC measurements performed with Al(99):Si(1) and W wires as reported in Tables II and III, the ratio of the radiation-dose measured by the 8 Ionization-Chambers I-C(1 → 8) is in agreement with the prediction of Eq. (1). In fact, taking into consideration the normalized radiation length of tungsten and aluminium [21]—0.35 and 8.89 cm, respectively—and the corresponding diameter of the wires—5 and 12.5 μm, respectively—according to Eq. (1) the ratio of the radiation-dose tungsten against

TABLE II. Radiation-dose—averaged over 10 scans and integrated over 30 beam shots—measured in different positions of the FERMI machine when scanning the electron beam—700 pC at 1.325 GeV—with a 12.5 μm Al(99):Si(1) wire and a 5 μm tungsten wire at a motor speed of 0.2 mm/s. The ratio—W against Al(99):Si(1)—of the measured radiation-dose is also shown. Absolute and relative measurements of radiation-dose have been performed with different detectors located at different positions of the machine. An absolute measurement of the radiation-dose rate (mGy/h) released on the FEL1 undulator chain is obtained by a set of 8 Ionization-Chambers (I-Cs) located in front, behind and in between the 7 undulator composing the FEL1 undulator chain. A relative measurement of the radiation-dose release in the FEL1 undulator chain is also obtained by means of 2 Cerenkov fibers—Cerenkov(1,2)—which are stretched along the FEL1 vacuum chamber. Finally, a further relative radiation-dose measurement is achieved by means of the scintillator fiber—BLM(1)—placed at 2.48 m from the WSC.

	I-C($1 \rightarrow 8$)(mGy/h)	Cerenkov(1)(arb.units)	Cerenkov(2)(arb.units)	BLM(1)(arb.units)
W(5 μm)	18.52 ± 1.31	$(5.18 \pm 0.26) \times 10^5$	$(1.00 \pm 0.05) \times 10^6$	1203 ± 70
Al:Si(12.5 μm)	1.65 ± 0.14	$(6.41 \pm 0.36) \times 10^4$	$(1.75 \pm 0.09) \times 10^5$	275 ± 15
Ratio(W/Al:Si)	11.2	8.1	5.7	4.4

aluminium is expected to be equal to $\frac{5}{12.5} \times \frac{8.89}{0.35} = 10.2$. This analysis of the experimental data acquired by the 8 Ionization-Chambers I-C($1 \rightarrow 8$)—as reported in Tables II and III—is consistent with the interpretation of similar experimental data already shown in Table I and previously discussed. As already commented in relation to the analysis of the experimental data in Table I, contrary to the BLM placed in a drift space at a distance of only 2.48 m from the WSC, the 8 Ionization-Chambers I-C($1 \rightarrow 8$) in the FEL1 undulator chain of FERMI are mainly sensitive to the high energy—and small scattering angle—component of the wire signal that is more likely transported through the entire vacuum chamber of the machine by the magnetic optics. Consequently, the relative ratio—tungsten against Al(99):Si(1)—of the radiation-dose measured by the 8 Ionization-Chambers I-C($1 \rightarrow 8$)—about a factor 11, see Table III—can be estimated by means of Eq. (1) that predicts a factor 10.2 as previously shown. Finally, the observed mismatch between the radiation dose measured by Cerenkov1&2 in FEL1—see Tables II and III—can be probably attributed to a different level of the signal amplification for the two Cerenkov fibers and/or a different sensitivity of the two detectors.

A last comment about Eq. (1) and the application limits of such a formula. According to the experimental tests so far carried out, the formula in Eq. (1) can be considered to provide a phenomenological interpretation of the FERMI measurements. Further experimental tests are required for a generalization of such a formula to a most complete description of the beam energy losses in a WSC measurements. Nevertheless, the outcome of the FERMI experiments confirmed the utility of such a formula that, thanks to the simplicity of the numerical implementation, can offer an useful and prompt support to an experimentalist in order to evaluate—on the basis of a simple rule-of-thumb criterion—the most suitable material for a given WSC application. An empirical justification of the formula in Eq. (1)—which only accounts for the contribution of the longitudinal thickness of the wire to the beam energy losses—comes from the circumstance that its predictions fit in a satisfactory way with the measurements of those beam loss monitors—such as BLM(2) and BLM(3) and the 8 I-Cs of the FEL1 undulator chain of FERMI, see Tables I–III—which in FERMI can only detect an energy selected fraction of the particle shower produced by the wire. The aforementioned detectors are placed at a large distance from the WSC and with many magnetic elements (dipoles, quadrupoles, steerings) in between. BLM(1) is conversely placed in a drift space from the WSC without any magnetic element in between. As a function of the energy acceptance of the series of magnetic elements placed between the WSC and the beam loss monitor, the fraction of the wire particle shower which can be transported along the beam pipe and finally detected by the BLMs is the result of an energy selection of the primitive particle shower. Only primary electrons scattered by the wire and secondary emitted electrons with an energy distribution matching the energy acceptance of the beam line from the WSC up to the FEL1 undulator line can be indeed detected by the 8 Ionization Chambers (I-Cs) placed

TABLE III. Ratio—W against Al(99):Si(1)—of the radiation-dose measured by three different detector when scanning the electron beam—700 pC at 1.325 GeV—with a 12.5 μm Al(99):Si(1) wire and a 5 μm tungsten wire at motor-speeds of 0.1, 0.2 and 0.3 mm/s. Radiation-dose measurements are performed: by a set of 8 Ionization-Chambers (I-Cs) located in front, behind and in between the 7 undulator composing the FEL1 undulator chain; by 2 Cerenkov fibers—Cerenkov(1,2)—which are stretched along the FEL1 vacuum chamber; finally, by a scintillator fiber—BLM(1)—placed at 2.48 m from the WSC.

	motor-speed(mm/s)	I-C($1 \rightarrow 8$)	Cerenkov(1)	Cerenkov(2)	BLM(1)
Ratio(W/Al:Si)	0.1	11.1	8.2	5.7	4.3
Ratio(W/Al:Si)	0.2	11.2	8.1	5.7	4.4
Ratio(W/Al:Si)	0.3	10.6	7.5	5.8	4.3

along the FERMI FEL1 undulator chain. The correspondence between the numerical predictions of Eq. (1)—only accounting for the contribution of the longitudinal wire size to the energy distribution of the wire particle shower—and the measurements of those beam-loss-monitors which detect an energy selected fraction of the wire particle shower can be considered an empirical justification of a formula which presently only aims at a phenomenological interpretation of the FERMI measurements.

In conclusion, the experimental tests of the SwissFEL WSC carried out at FERMI—at the GeV energy scale and at high beam charge—gave an answer to several questions of the design of the SwissFEL WSC. Two possible wire-material solutions for the SwissFEL WSC (12.5 μm Al(99):Si(1) and 5 μm W wires) were tested at FERMI and both of them demonstrated a suitable beam robustness. The optimum distance of the BLM from the WSC was estimated between 5 and 6 m at the GeV energy scale (at FLASH, an optimum distance WSC-BLM of about 4.8 m was estimated [13]). The new metallic wire solution—Al(99):Si(1)—proposed as an alternative to the traditional tungsten solution showed a very good performance in terms of reduction of the radiation-dose release. Compared to a scan with a 5 μm W wire, a drastic reduction—by a factor 11—of the radiation-dose along the machine when scanning the beam with a 12.5 μm Al(99):Si(1) was indeed observed. Finally, the WSC test at FERMI demonstrated that the same accuracy can be achieved by the 12.5 μm Al(99):Si(1) and 5 μm W wires in measuring a beam size of about 35 μm. Furthermore, this measurement accuracy was observed to remain constant—within the limit of the statistical errors—in the motor-speed range between 0.1 and 0.3 mm/s. The extrapolation of this result to the case of SwissFEL—repetition rate of 100 Hz, i.e., 10 times higher than FERMI—indicates that a sufficiently precise and machine-saving monitoring of a beam profile with a size of 35 μm can be still performed at SwissFEL with a 12.5 μm Al(99):Si(1) wire at a motor speed of 3.0 mm/s.

III. CONCLUSIONS

The design features and the main prototyping steps of the SwissFEL wire scanners have been presented as well as the results of bench and electron-beam tests of the entire WSC setup. Electron beam tests were carried out at SITF and FERMI. The experimental characterization of the mechanical stability of the WSC confirmed that, in the motor-speed range of interest of SwissFEL (0.1–3.0 mm/s), the wire-vibration stays largely below the tolerance limit of 1.3 μm (rms). According to the results of electron beam tests carried out at SITF, the detection setup of the wire signal showed a sufficient sensitivity to reconstruct the beam profile of a 10 pC beam scanned by a 5 μm tungsten wire and, in general, a sufficient large dynamics to cover the beam charge range 10–200 pC. Furthermore, thanks to the electron beam tests carried out at SITF and FERMI, the optimum distance between WSC and wire-signal detector was estimated to scale up between 3 and 6 m in the beam energy range 0.250–1.5 GeV. Several solutions of metallic wires of different material and diameter have been tested on the electron beam at different conditions of charge and energy. In particular, comparative tests of the scanning performance of a 5 μm tungsten wire and of 12.5 μm Al(99):Si(1) wire were carried out at FERMI at a beam energy of 1.325 GeV and charge of 700 pC. The results of this comparative study demonstrated a satisfactory robustness of the Al(99):Si(1) wire to the beam loading as well as a comparable accuracy of the two wire-solutions in measuring an electron beam size of about 35 μm. In addition, the radiation-dose measured at the FEL1 undulator chain of FERMI when scanning the beam with a 12.5 μm Al(99):Si(1) was about a factor 11 smaller than the one measured with a 5 μm tungsten wire. On the basis of the outcome of the electron beam tests, the SwissFEL WSC forks—being designed to be equipped with two distinct triplets of metallic wires—will be provided with 5 μm tungsten wires—for high precision measurements of the beam profile and emittance—and with 12.5 μm Al(99):Si(1) wire for routine monitoring of the transverse profile of the electron beam during FEL operations. The prototyping and experimental characterization phases of the SwissFEL WSC being accomplished, WSC commissioning and operations in SwissFEL are expected to start by Summer 2016.

ACKNOWLEDGMENTS

The authors wish to thank the Paul Scherrer Institut expert groups, the SITF commissioning team and the FERMI operation crew for the support during the measurements. In particular, the authors are grateful to: M. Baldinger (PSI), B. Rippstein (PSI), M. Magiar (PSI), N. Gaiffi (PSI), L. Schulz (PSI), A. Zandonella (PSI) for mechanics and vacuum; C. Pradervand (PSI) for motion control standardization; K. Bitterli (PSI), H. Brands (PSI), T. Celcer (PSI), S. Ebner (PSI), B. Kalantari (PSI), D. Maier-Manojlovic (PSI), T. Zamofing (PSI), D. Zimoch (PSI), E. Zimoch (PSI), T. Slejko (COSYLAB), T. Sustar (COSYLAB) and R. Vintar (COSYLAB) for controls; P. Pollet (PSI) for designing the BLM electronics; P. Mohanmurthy (PSI) for collaborating as a summer student to WSC prototyping; P. Ming (PSI), J. Wickstroem (PSI) and P. Fischer (PSI) for quality control, logistics and contract-management; F. Löhl (PSI), R. Dölling (PSI), R. Ganter (PSI), R. Lüscher (PSI), M. Pedrozzi (PSI) and H. H. Braun (PSI) for useful discussions and comments on WSC design and results; L. Sturari (FERMI) and R. Sauro (FERMI) for the installation and alignment on FERMI; S. Grulja (FERMI) for integrating the SwissFEL WSC in the FERMI control system and G. Gaio (FERMI) for the data acquisition integration; S. Di Mitri (FERMI) and L. Giannessi (FERMI) for useful discussions and comments on results.

[1] SwissFEL Conceptual Design Report No. PSI Bericht Nr. 10-04, 2012.

[2] P. Emma, J. Frisch, and P. Krejcik, Report No. LCLS-TN-00-12.

[3] Z. Huang and K. J. Kim, Phys. Rev. ST Accel. Beams **5**, 074401 (2002).

[4] E. L. Saldin, E. A. Schneidmiller, and M. V. Yurkov, Nucl. Instrum. Methods Phys. Res., Sect. A **528**, 355 (2004).

[5] R. Fulton, J. Haggerty, R. Jared, R. Jones, J. Kadyk, C. Field, W. Kozanecki, and W. Koska, Nucl. Instrum. Methods Phys. Res., Sect. A **274**, 37 (1989).

[6] M. C. Ross, J. T. Seeman, E. Bong, L. Hendrickson, D. McCormick, and L. Sanchez-Chopitea, in *Proceedings of the 1991 Particle Accelerator Conference, San Francisco, CA, 1991* (IEEE, New York, 1991).

[7] C. Field, Nucl. Instrum. Methods Phys. Res., Sect. A **360**, 467 (1995).

[8] P. Tenenbaum and T. Shintake, Annu. Rev. Nucl. Part. Sci. **49**, 125 (1999).

[9] H.-D. Nuhn, P. J. Emma, G. L. Gassner, C. M. LeCocq, F. Peters, and R. E. Ruland, Report No. SLAC-PUB-12098, 2006.

[10] H. Loos *et al.*, Report No. SLAC-PUB-14121.

[11] J. Wu, P. Emma, and R. C. Field, Report No. SLAC-PUB-12120 LCLS-TN-06-7, 2006.

[12] K. Wittenburg, Report No. TESLA2000-18, 2000.

[13] U. Hahn, N. v. Bargen, P. Castro, O. Hensler, S. Karstensen, M. Sachwitz, and H. Thom, Nucl. Instrum. Methods Phys. Res., Sect. A **592**, 189 (2008).

[14] R. Ischebeck, E. Prat, V. Thominet, and C. Ozkan Loch, Phys. Rev. ST Accel. Beams **18**, 082802 (2015).

[15] C. Ozkan Loch, D. Llorente Sancho, P. Pollet, G. Marinkovic, R. Ischebeck, and V. Schlott, System Integration of SwissFEL Beam Loss Monitors, in *Proceedings of IBIC2015, Melbourne, Australia (MOPB051), 2015*, pp. 170–174.

[16] B. Keil, R. Baldinger, R. Ditter, D. Engeler, W. Koprek, R. Kramert, A. Malatesta, F. Marcellini, G. Marinkovic, M. Roggli, M. Rohrer, and M. Stadler, Status of the SwissFEL BPM System, in *Proceedings of IBIC2015, Melbourne, Australia (TUPB065), 2015*, pp. 497–501.

[17] SwissFEL Injector Conceptual Design Report, PSI Bericht Nr. 10-05, 2010.

[18] C. Bocchetta *et al.*, FERMi@Elettra Conceptual Design Report, Tech Report No. ST/F-TN-07/12, 2007.

[19] S. Di Mitri, E. Allaria, L. Badano, C. Bontoiu, M. Cornacchia, P. Craievich, M. Danailov, G. De Ninno, B. Diviacco, O. Ferrando, S. Ferry, F. Iazzourene, S. V. Milton, G. Penco, S. Spampinati, M. Trovò, M. Veronese, W. Fawley, S. Lidia, G. Penn, J. Qiang *et al.*, Nucl. Instrum. Methods Phys. Res., Sect. A **608**, 19 (2009).

[20] The square rms size of a cylindrical wire (diameter D) reads: $\sigma_{rms}^2 = \frac{\int_{-D/2}^{D/2} x^2\sqrt{(D/2)^2-x^2}dx}{\int_{-D/2}^{D/2}\sqrt{(D/2)^2-x^2}dx} = D^2/16$.

[21] R. C. Fernow, *Introduction to Experimental Particle Physics* (Cambridge University Press, Cambridge, England, 1986).

[22] T. Moore, N. I. Agladze, I. V. Bazarov, A. Bartnik, J. Dobbins, B. Dunham, S. Full, Y. Li, X. Liu, J. Savino, and K. Smolenski, Phys. Rev. ST Accel. Beams **17**, 022801 (2014).

[23] H. Akikawa, Z. Igarashi, M. Ikegami, S. Lee, Y. Kondo, S. Sato, T. Tomisawa, and A. Ueno, in *Proceedings of the 23rd International Linac Conference, LINAC-2006, Knoxville, TN, 2006* (JACoW, Knoxville, TN, 2006).

[24] J. Herranz, A. Barjau, and B. Dehning, Mechanical Systems and Signal Processing **70–71**, 974 (2016).

[25] P. Mohanmurthy, G. L. Orlandi, and R. Ischebeck, in *2012 Fall Meeting of the APS Division of Nuclear Physics*, http://meetings.aps.org/link/BAPS.2012.DNP.EA.74.

[26] G. L. Orlandi, M. Baldinger, H. Brands, P. Heimgartner, R. Ischebeck, A. Kammerer, F. Löhl, R. Lüscher, P. Mohanmurthy, C. Ozkan, B. Rippstein, V. Schlott, L. Schulz, C. Seiler, S. Trovati, P. Valitutti, and D. Zimoch, Design and test of Wire-scanners for SwissFEL, in *Proceedings of FEL2014, Basel, Switzerland (THP091), 2014*, pp. 948–951.

[27] A. Ferrari, P. R. Sala, A. Fassò, and J. Ranft, Reports No. CERN-2005-10, 2005, No. INFN/TC_05/11, No. SLAC-R-773.

[28] S. Trovati, PSI Internal Note Report No. FEL-TS96-001-0.

[29] E. Hohmann, S. Reiche, A. Fuchs, R. Ganter, F. Le Pimpec, R. Lüscher, S. Mayer, and T. Schietinger, Prog. Nucl. Sci. Technol. **4**, 762 (2014).

[30] G. Penco, G. L. Orlandi, M. Ferianis, E. Ferrari, G. Gaio, and C. Ozkan Loch (to be published).

[31] E. Allaria *et al.*, Nat. Photonics **6**, 699 (2012).